

Multichannel Dosimeter and α-Al_2O_3:C Optically Stimulated Luminescence (OSL) Fiber Sensors for Use in Radiation Therapy-Evaluation With Photon Beams

Sylvain Magne, Loïc de Carlan, jean-marc bordy, Aurélie Isambert, André Bridier, Pierre Ferdinand

▶ **To cite this version:**

Sylvain Magne, Loïc de Carlan, jean-marc bordy, Aurélie Isambert, André Bridier, et al.. Multichannel Dosimeter and α-Al_2O_3:C Optically Stimulated Luminescence (OSL) Fiber Sensors for Use in Radiation Therapy-Evaluation With Photon Beams. IEEE Transactions on Nuclear Science, 2011, 58 (2), pp.386 - 394. 10.1109/TNS.2011.2114369 . cea-01840719

HAL Id: cea-01840719
https://cea.hal.science/cea-01840719

Submitted on 16 Jul 2018

HAL is a multi-disciplinary open access archive for the deposit and dissemination of scientific research documents, whether they are published or not. The documents may come from teaching and research institutions in France or abroad, or from public or private research centers.

L'archive ouverte pluridisciplinaire **HAL**, est destinée au dépôt et à la diffusion de documents scientifiques de niveau recherche, publiés ou non, émanant des établissements d'enseignement et de recherche français ou étrangers, des laboratoires publics ou privés.

Multichannel Dosimeter and α-Al_2O_3:C Optically Stimulated Luminescence (OSL) Fiber Sensors for Use in Radiation Therapy—Evaluation With Photon Beams

Sylvian Magne, Loïc de Carlan, Jean-Marc Bordy, Aurélie Isambert, André Bridier, and Pierre Ferdinand

***Abstract*—A multichannel OSL fiber optic dosimeter based on optically stimulated luminescence (OSL) of alumina is proposed for online *in vivo* dosimetry (IVD) in radiation therapy (RT). Two types of dosimetric-grade Al_2O_3 : C crystals are compared and show different behavior according to manufacturing process. Metrological validations have been performed with a Saturne 43 LINAC in reference conditions at CEA LIST LNHB (French Ionizing Radiation Reference Laboratory). The dose response of OSL integrals under photon beam irradiation (6, 12, and 20 MV) show sublinearity behavior modeled by second-order equations and exhibit a small energy dependence (between 0.7% and 1.4%), explained by a modified intermediate cavity model adapted to a LINAC photon spectrum. Preclinical tests at Institut Gustave Roussy (IGR) prove that a proper design for a PMMA build-up cap leads to a low dependence vs photon beam orientation ($\pm$1.5% and $\pm$0.9%) and vs field size in view of surface measurements.**

***Index Terms*—*In Vivo* Dosimetry (IVD), Optical Fiber Sensor (OFS), Optically Stimulated Luminescence (OSL), radiotherapy.**

I. Introduction

THE CEA LIST works on optically stimulated luminescence dosimetry (OSLD) since 1993, essentially with rare-earth (RE) doped II-VI polycrystals (e.g., MgS: Ce, Sm) and alumina crystals as OSL materials. A first-generation fiber optic OSL dosimeter (OSL/FO I) was developed using RE-doped II-IV polycrystals (provided by the University of Montpellier, France), that consisted in a fiber sensor affixed to a strand of fiber (50-meter long) and connected to an industrial computer [1]. Several OSL/FO I systems were sold to AREVA NC (formerly COGEMA) and to CEA (Marcoule Research Center, France) and used for radioactive clean-up of out-of-reach areas (pipes, tanks, etc.) prior to dismantling [2]. These RE-doped II-VI polycrystals are sensitive OSL materials, suitable for long-range detection owing to near infrared optical stimulation. However, they are not tissue-equivalent and plagued with high OSL fading that necessitates a complicated time- and temperature-dependent correction. Moreover, they are not optically transparent and thus mostly used for surface imaging applications.

Since 1998, the CEA LIST investigated dosimetric-grade alumina crystals α-Al_2O_3:C in a purpose of radiation protection. These crystals (grown in reducing atmosphere in the presence of carbon) convey a lot of advantages (high sensitivity, large dynamic range, small fading at room temperature, low Z, etc.) [3]. Alumina pellets or fibers are available at low cost. High active volume (mm^3 or cm^3) may be used owing to optical transparency of alumina thus increasing the output signal from the device. A dose limit of 20 μGy was achieved with a 20-meter-long Al_2O_3-OSL fiber sensor, linked to a second-generation OSL/FO system (OSL/FO II) [4]. Since then, significant progress was made in the technology (laser power, data processing) so that this dose limit is likely to be substantially improved.

From 2004 to 2009, the CEA LIST managed the European Project MAESTRO, dedicated to the development of technologies and treatment techniques in radiation therapy (RT) [5]. This project involved several cancer research institutes and hospitals among which the Institut Gustave Roussy (IGR), as centre of expertise.

Today, about 60% of all cancer patients are treated by RT alone or in combination with surgery or chemotherapy. Most RT treatments involve photon or electron beams delivered by linear accelerators (LINACs). Electron beams are used to treat superficial or shallow tumors close to the skin surface. Photon beams however penetrate more deeply within the human body and overlap significantly with healthy tissues. Therefore, a combination of several beams adequately oriented allows the radiation oncologist to deliver the prescribed dose to the target volume without exceeding the tolerance for surroundings healthy tissues and organs at risk and thus reduce undesirable complications. The so-called intensity-modulated RT (IMRT) improves the conformity of the dose distribution to the tumor but, in return, it brings additional complexity and processing time in the dosimetry due to high-dose gradients and more complex ballistics.

Manuscript received June 26, 2009; accepted February 02, 2011. Date of publication March 10, 2011; date of current version April 13, 2011. This work was supported in part by the European Commission (MAESTRO Project CE503564 [Methods and Advanced Equipments for the Simulation and Treatment in Radio Oncology] of the Sixth Framework Program) and by the Agence Nationale pour la Recherche-Technologies pour la Santé (ANR-TECSAN CODOFER).

S. Magne and P. Ferdinand are with the CEA, LIST, Laboratoire de Mesures Optiques, F-91191 Gif-sur-Yvette, France (e-mail: sylvain.magne@cea.fr).

L. de Carlan and J. M. Bordy are with the CEA, LIST, Laboratoire National Henri Becquerel, F-91191 Gif-sur-Yvette, France (e-mail: jean-marc.bordy@cea.fr).

A. Isambert and A. Bridier are with the Institut Gustave Roussy, Service de Physique, F-94805 Villejuif, France (e-mail: bridier@igr.fr).

Color versions of one or more of the figures in this paper are available online at http://ieeexplore.ieee.org.

Digital Object Identifier 10.1109/TNS.2011.2114369

0018-9499/$26.00 © 2011 IEEE

Treatment planning systems (TPS) are used to plan the treatment. Severe accidents in RT have been associated with the incorrect use of TPS or false dose measurement during its commissioning. *in vivo* dosimetry (IVD) is an additional safeguard against major set-up, dose calculation and transfer errors that could have been missed when only a pre-treatment verification was performed. IVD is now a legal requirement in France as it will be mandatory by 2011. It has to be used at least at the beginning of a new treatment and whenever any change occurs in the treatment planning. According to the Code of Practice (CoP) IAEA TRS-398 [6] the difference between planned and delivered doses must remain within typically 2% to 3%. If the difference exceeds 5%, the reasons for discrepancy must be investigated and the patient treatment should not be initiated.

In external beam RT, dosimeters are placed on the patient's skin. Practically, they are mounted into a build-up cap that puts the dosimeter in local electronic equilibrium condition, most often at the position of dose maximum $(\mathrm{d_{max}})$. The main advantage of this configuration lies in the low placement-induced uncertainty due to the low dose gradient near $\mathrm{d_{max}}$. Furthermore, the shape of the cap may be tailored to provide angular independence which is also a strong request from medical physicists as the dosimeter orientation with respect to irradiation beam is likely to change depending on its placement along the patient's body. The dose to the tumor is then inferred from surface measurement taking into account the dose distribution given by the TPS, the maxima of dose respectively calculated by the TPS and measured (at $\mathrm{d_{max}}$).

IVD is traditionally provided by thermoluminescent dosimeters (TLDs), metal-oxide semiconductor field-effect transistors (MOSFETs) or PN-junction-type diodes. Ionization chambers (ICs) are considered as absolute dosimeters but are not routinely used on account on their large size and the use of high voltage. MOSFETs have a limited lifetime due to the saturation of threshold voltage ($\sim$200 Gy), must be frequently recalibrated and show high fading. TLDs necessitate a complex and time-consuming protocol (annealing). These methods do not provide real-time dose monitoring on a routine basis and are costly. Only diodes are widely used in clinical routine on account of their small size and sensitivity and also real-time monitoring capability. However, the cable is not radiation-transparent and disturbs the radiation field. Moreover, several correction factors have to be applied for dose calculation (temperature, dose rate (source-to-surface distance), angular and energy dependencies). The dose sensitivity depends on radiation history and periodic recalibrations are necessary.

It is worthwhile to note that OSL IVD with Al_2O_3:C crystals is recently gaining acceptance from the medical community [7]–[11]. The principles of OSL are described in many papers [4]–[7] and will not be reviewed here. Recent clinical investigations were conducted with InLight Dot dosimeters (associated to the MicroStar reader) or Luxel films, collected after irradiation and mailed to Landauer Inc. (Glenwood, IL) for readout. Since the optical readout does not bleach the OSL film, it can be stored and read at a later date.

However, in clinical conditions, medical physicists are willing to save time at the dosimetry stage. Furthermore, an immediate readout after treatment is desirable in order to reduce the inter-patient time and also to provide suitable action in case of abnormal dose delivery. The real-time monitoring of the cumulated doses may be also mandatory for specific treatments [e.g., total body irradiation (TBI), total skin electron therapy (TSET)] and may be obtained from real-time OSL or radioluminescence (RL) of Al_2O_3:C crystals.

For this purpose, several research groups have investigated fiber sensing solutions for online remote dose measurement in RT, mostly with Al_2O_3:C crystals [12], [13] as parallel developments to ours [14]. The OSL/FO reader of the CEA LIST has the capability of measuring the dose rate during treatment (time-sampling by the optical switch) and the dose after treatment, without necessity for disconnecting the sensor (online readout). The objective is to provide an accurate, cost-effective, efficient and reliable IVD to fulfill the quality assurance in RT while keeping operational costs at a reasonable level. Our main innovation lies in the multichannel capability in a purpose of cost effectiveness (low cost/sensor figure) and easier data acquisition and archiving.

In [14], we investigated OSL/FO sensors in megavoltage (MV) electron beams typically used for RT treatments. We concluded that it was necessary to irradiate them (up to 200 Gy) prior to use. The predose fills the deep traps that are not emptied by optical stimulation thus stabilizing the sensor response. Once predosed (only once), they show repeatability in multichannel operation better than $\pm 1\%$, demonstrating the reliability of the switching mechanism as well. The energy dependence of the dose response is small ($\pm 0.25\%$ over [9 MeV, 18 MeV]) due to smallness of the OSL crystal (Bragg–Gray cavity theory). Depending on the readout procedure, the temperature coefficient of the OSL signal lies between $0.3\%.\mathrm{K}^{-1}$ and $0.16\%.\mathrm{K}^{-1}$. Practically, the uncertainty in surface temperature is typically $\pm 2^{\circ}$C. Therefore, the uncertainty in dose measurement due to temperature fluctuations is likely to be about $\pm 0.3\%$, still acceptable for IVD purpose.

In [15], we also demonstrated that a dedicated build-up cap also provides angular independence. The variation in dose measurement was of same order than repeatability ($\pm 1\%$) when the dosimeter was rotated within the range [0°, 45°] in both directions (i.e., within a plane perpendicular to fiber axis and within a plane containing fiber axis). Electron beams were used for this experiment.

Finally, in the context of an ever-increasing complexity of the radiation treatments, the purpose is also to save time in calibration and maintenance. Radiation-hard dosimeters with long-term stability of their dose response are desirable in order to avoid frequent time-consuming and costly recalibrations. We have shown that OSL/FO sensors can withstand dose level as high as 60 kGy [15]. This amount of dose is equivalent to a three-year period of day-to-day RT treatments (2 Gy per treatment, 4 treatments per hour). The reproducibility in dose measurements was kept at $\pm 2\%$ during this experiment that demonstrates that OSL sensors are less prone to radiation damage than semiconductor dosimeters (diodes) and consequently less costly in consumable (longer lifetime). It is worth noticing that the sensor survived the test.

In this paper, we describe the metrological validations of OSL/FO sensors performed at CEA-LNHB (Laboratoire

National Henri Becquerel), the French National Metrology Laboratory for ionizing radiation, and preclinical tests of such sensors done at IGR for use in external-beam RT with photon radiation.

II. OSL/FO Multichannel Dosimeter

A. OSL/FO Reader

The OSL/FO reader was already described in previous publications [14], [15]. It is built in a 19-inch enclosure (6U) that includes a 16-channel optical fiber switch actuated by a stepper motor, an optical case containing a green-emitting laser, optoelectronics detection devices and power/USB electronics. The reader is linked to a laptop by an USB connection and handled through dedicated software written in LabView. During experiments with LINACs, the reader is located in the control room (next to the irradiation room) and fiber cables run through the wall (length: 28 m).

After irradiation, each sensor is remotely stimulated using a CW-diode-pumped solid-state (DPSS) laser (@532 nm, 200 mW) and bleached for a next use. The reader works in the continuous-wave mode (CW-OSL). The OSL stimulation is triggered by an electromagnetic shutter once the switch has moved from its reference position to the selected output. The OSL (@410 nm) is then collected by the optical fiber, separated by a dichroïc beam splitter, filtered and eventually detected by a photomultiplier in photon-counting mode. The data counts are corrected for counter dead-time influence (20 ns). The background signal is also averaged from the latest portion of the OSL signal and subtracted from the raw signal. The resulting OSL curve is finally integrated and multiplied by a calibration coefficient to provide the absorbed dose.

Several autotests are included into the software that controls every critical device (laser, photo-multiplier and counting electronics, switch, acquisition board). The global measurement chain is tested using a fluorophore and the amount of fluorescence light is compared to laser power and also corrected for ambient temperature variations.

B. OSL Fiber Sensors

Al_2O_3:C OSL/FO sensors are made with polymers and use silica fibers. They are nearly radiation-transparent and do not interfere with radiation field. They are also compatible with *in vivo* applications (small size, non-toxic, chemically inert and sterilizable) and electromagnetic-immune.

We used the same OSL/FO sensor design as in [14] (Fig. 1). However, we investigated two dosimetric-grade alumina crystals provided by two manufacturers. The first alumina crystal is sold as fiber crystal under the trademark TLD_{500} and was purchased from Ural State Technical University (Ekaterinburg, Russia). The second alumina crystal was purchased as pellet from Landauer Inc. in 2000 (labeled as "Landauer" in this paper).

Each crystal was affixed onto the extremity of a fiber sensor: OSL#3 (TLD_{500}) and OSL#8 (Landauer). The readout time depends on trap distribution within the crystal and is thus strongly dependent on crystal manufacturing.



Fig. 1. OSL/FO sensor (top) and mounted with a PMMA build-up cap for surface measurements (bottom).

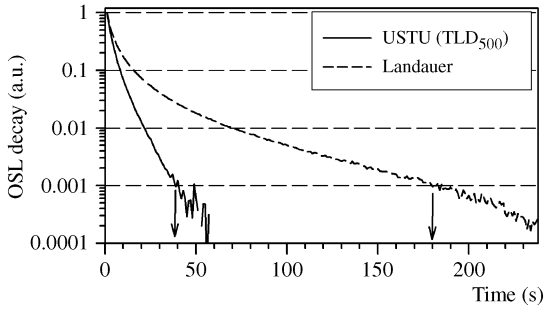


Fig. 2. OSL decay curves for TLD_{500} and Landauer crystals.

Fig. 2 shows the OSL decay curve (at room temperature and normalized to maximum) versus time for a laser power of ~35 mW at fiber end (~22 mW/mm^2). Let us consider three orders of magnitude in OSL signal reduction (−30 dB) as a comparison basis. One can see that the TLD_{500} crystal is optically bleached within 40 s while the Landauer crystal necessitates 180 s (3 minutes).

III. Fading Behavior

Previous experiments with Luxel dosimeters (Landauer Inc.) have shown a signal increase immediately after irradiation which precludes an immediate readout as a delay time of 6 to 7 minutes is necessary to get a stable OSL readout [9].

The fading behavior of Landauer crystals was investigated using a X-ray generator (80 kV) and compared to that of TLD_{500} [14] in the time scale [2 seconds, 2 hours]. Although both crystals have very different trap distributions, neither of them exhibit transient effect (Fig. 3). Therefore, both crystals may be used for online IVD.

IV. Metrological Validation With Photon Beams

A. Experimental

Irradiations were performed at CEA LIST LNHB. Calibrations were made with a Saturne 43 LINAC, according to the CoP TRS-398 [6] that involves a water cubic phantom (side length: 30 cm), a field size (FS) of 10×10 cm^2 and a source-to-surface distance (SSD) of 90 cm (see Fig. 4).

An IC is used for comparison. The dose rate was 200 MU/min (about 2 Gy/min) at a depth of 10 cm in water. Three reference energies E_{ref} were used: 6 MV, 12 MV, and 20 MV, corresponding to the following tissue phantom ratios ($TPR_{20,10}$): 0.675, 0.749, and 0.784, respectively.

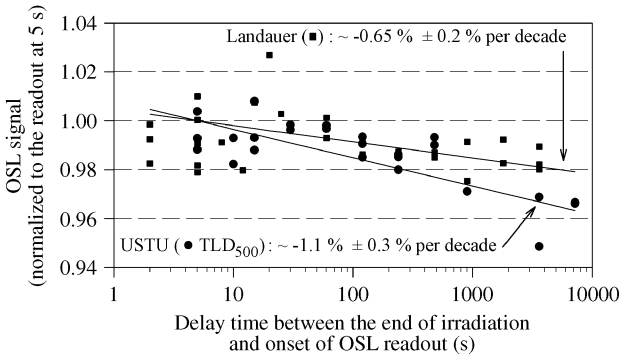


Fig. 3. Short-term fading behavior of both Landauer and TLD_{500} crystals.

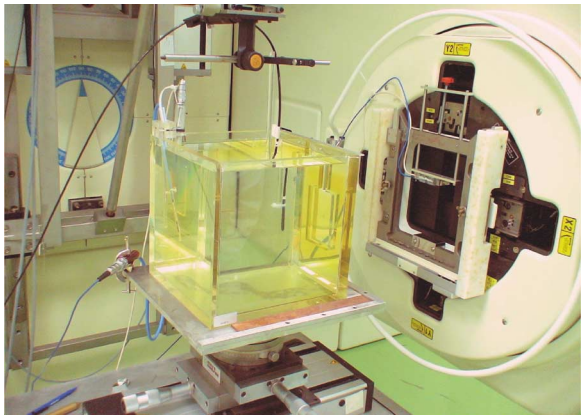


Fig. 4. Metrological validation in photon beam with a water cubic phantom (courtesy CEA LIST LNHB).

B. OSL Response With Dose

Both amplitude and integral of OSL signal may be used for dose monitoring. Both parameters were investigated for the two sensors (OSL#3 and OSL#8). However, the monitoring of the amplitude requires a more careful control of laser power.

Evolution of the Amplitude of OSL Signal Versus Dose: Fig. 5 shows the amplitude of OSL signals for both sensors for the three reference energies used. One can see that OSL amplitudes do not significantly depend on photon energy and behave very differently with respect to dose. The dose response of the TLD_{500} crystal is nearly linear until 1 Gy (departure of -3.3%) and then shows a small sub-linearity (-10% at 3 Gy). Conversely, the dose response of the Landauer crystal is strongly superlinear and then shows sublinearity for higher dose (>3 Gy). This typical figure-of-S behavior is also encountered with *Luxel* and *In-Light* dosimeters [16]. This difference is usually attributed to the high deep trap concentration in Landauer alumina crystals [17].

Evolution of the Integral of OSL Signal Versus Dose: By contrast, the evolutions of the OSL integrals for both crystals look much more similar and are modeled by a second-order equation as in [14]

$$a.D^2 - s.D + I_{\mathrm{OSL}} = 0. \quad (1)$$

The dose response of the OSL integral is shown in Fig. 6 for the TLD_{500} crystal and in Fig. 7 for the Landauer crystal. Second-order polynomial equations were adjusted according to

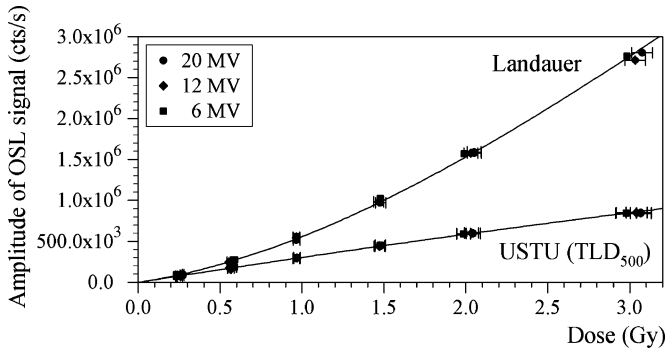


Fig. 5. Evolution of the amplitudes of OSL signals for OSL#3 (TLD_{500}) and OSL#8 (Landauer) for three reference energies (6 MV, 12 MV and 20 MV).

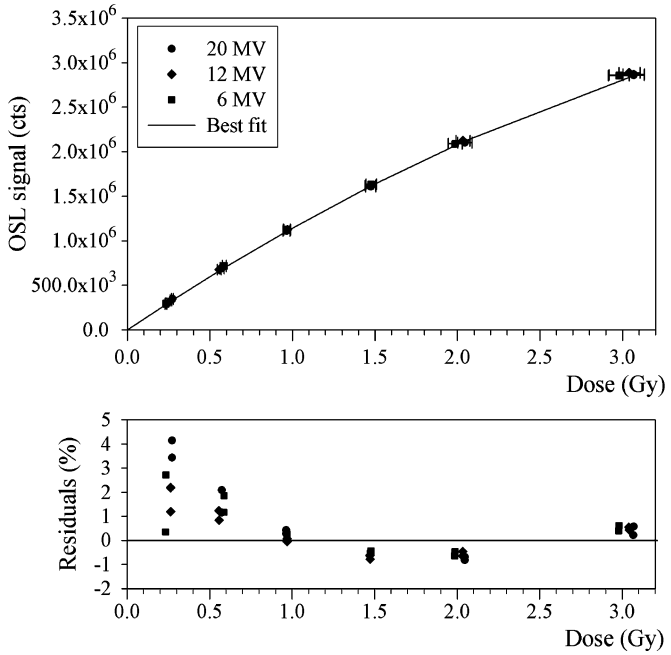


Fig. 6. (Top) Evolution of the integrals of OSL signals for OSL#3 (TLD_{500}) for the three reference energies (6 MV, 12 MV, and 20 MV). (Bottom) Relative difference (residuals) between OSL data and each fit equation associated to each reference energy.

least-square analysis. The residuals ($100 \times$ [OSL signal-fit]/fit) are plotted on bottom part of the figure. One can see that a third-order contribution remains that accounts for less than 1% of the dose response at high dose. This third-order contribution is of opposite sign depending on the crystal (i.e., depending on sublinearity or superlinearity behavior). The residuals are well superimposed and centered around 0%.

The fit parameters are listed in Tables I and II for TLD_{500} and Landauer crystals, respectively.

It is interesting to notice that the decay parameter for OSL signal of Landauer crystals increases with dose, i.e., the OSL decay curve narrows when increasing dose (laser power is kept constant). As a consequence of that, the OSL integrals of the Landauer crystal show a smaller superlinearity behavior than the amplitude does because superlinearity is partly compensated for by the time narrowing of the OSL signal. The departure from linearity is about -8% and -3.5% at 1 Gy for TLD_{500} crystals and Landauer crystals respectively.

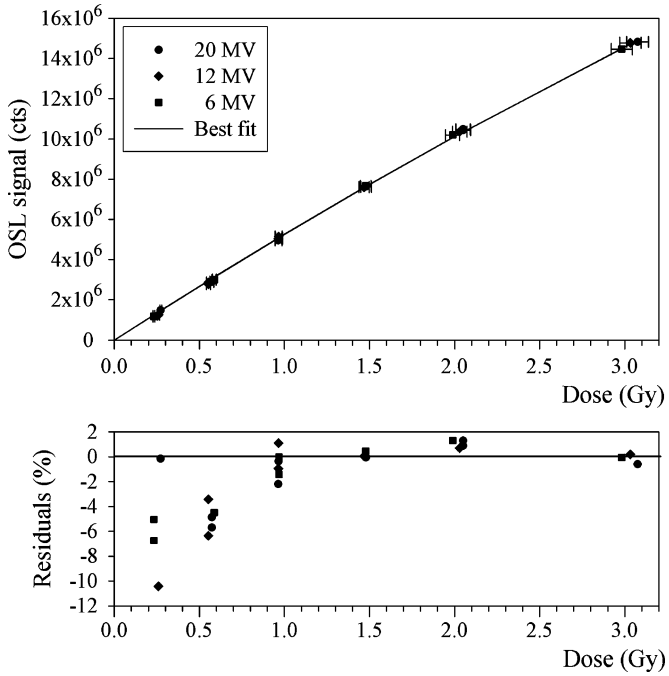


Fig. 7. (Top) Evolution of the integral of OSL signals for OSL#8 (Landauer) for the three reference energies (6 MV, 12 MV, and 20 MV). (Bottom) Relative difference (residuals) between OSL data and each fit equation associated to each reference energy.

TABLE I
CALIBRATION PARAMETERS FOR OSL INTEGRAL (TLD_{500})

Photon energy	6 MV	12 MV	20 MV
s (10^6 cts/Gy)	1.267 ± 2.10^{-3}	1.262 ± 2.10^{-3}	1.249 ± 2.10^{-3}
a (10^3 cts/Gy^2)	105 ± 5	104.5 ± 5	104 ± 5

TABLE II
CALIBRATION PARAMETERS FOR OSL INTEGRAL (LANDAUER)

Photon energy	6 MV	12 MV	20 MV
s (10^6 cts/Gy)	5.48 ± 10^{-2}	5.47 ± 10^{-2}	5.44 ± 10^{-2}
a (10^3 cts/Gy^2)	210 ± 10	200 ± 10	192 ± 10

Equation (1) is valid for $D < D_{\mathrm{M}} = (\mathrm{s}/2.\mathrm{a})$ which sets the dose range as 6 Gy for TLD500 crystals and 13 Gy for Landauer crystals.

C. Energy Dependence in Reference Conditions

As can be seen in Tables I and II, the dose response of the OSL sensor relative to that of water exhibits a dependence—albeit small—with respect to photon energy of about 1.4% and 0.7% over [6 MV, 20 MV] for TLD_{500} and Landauer crystals respectively (uncertainty $\sim \pm 0.2\%$).

The energy dependence of OSL sensors is more pronounced with MV photon beams than with MV electron beams [14] because the energy spectra are very different. Indeed, the spectrum of the electron beam exiting the LINAC head (say, at a distance in air of 1 m) is still roughly monochromatic despite the straggling effect due to scattering foils [18]. It looks roughly like a Gaussian distribution of peak energy approximately 90% of reference energy. The electron spectrum then progressively degrades as the electron beam penetrates through water. On the contrary, the *Bremsstrahlung* spectrum S(E) of the photon beam exiting the LINAC head (resulting from the interaction on the primary electron beam onto the conversion target) is spread over $[0,\ E_{\mathrm{ref}}]$. Consequently, the mean energy and spectral width of the photon spectrum are respectively much lower and larger than those of the original electron spectrum. As a usual rule of thumb, the peak energy (i.e., maximum fluence) roughly equals $E_{\mathrm{ref}}/4$ to $E_{\mathrm{ref}}/5$ depending on LINAC technologies. The photon fluence progressively decreases as the photon beam penetrates through water but the photon spectrum remains roughly constant (let alone contamination by low-energy scattered photons).

Compton scattering effect is the prominent interaction mode for photons within the energy range [50 keV, 24 MeV] for silica fibers or alumina crystals ($\mathrm{Z_{eff}} \sim 11$). Within this interaction mode, an initial photon of energy $\mathrm{h}.\nu_0$ is scattered by an electron so that the photon has a degraded energy $\mathrm{h}.\nu$ and the recoil electron has acquired a kinetic energy equal to the remaining part $(\mathrm{h}.(\nu - \nu_0))$.

The average starting kinetic energy of the Compton recoil electrons can be written as [19]

$$\overline{T} = h.\nu_0.\frac{\sigma_a}{\sigma_t} \tag{2}$$

where σ_{a} and σ_{t} are the absorption Compton cross-section and interaction Compton cross-section, respectively. The ratio $\sigma_{\mathrm{a}}/\sigma_{\mathrm{t}}$ corresponds physically to the fraction of incident photon energy delivered to recoil electrons. This fraction is given in many books [19], [20].

This calculation is based upon the assumption that the probability for double-scattering event is negligible. Since the volume of alumina crystal is small (mm^3), the probability for scattering event within the crystal is about 1% to 2% depending on reference energy. Therefore, the probability for double-scattering event is less than 0.04% and only one event is assumed for each initial photon. For low photon energy (<50 keV), the Compton cross-section is reduced due to electron binding effect but practically it is largely compensated for by photoelectric interaction.

Nowadays, these problems are often solved by Monte-Carlo calculations. However, it is still possible to get a theoretical estimate of the energy dependence of the absorbed dose inside the dosimeter (i.e., OSL crystal) with respect to the dose in reference medium (water). The mean range of Compton electrons lies between 0.3 g/cm^2 up to 1 g/cm^2 in the energy range [6 MV, 20 MV] [21]. In water, it lies between 4 mm and 8 mm while in alumina (3.97 g/cm^3), it lies between 1 and 2 mm and is thus of same order as to the size of both alumina crystal and polymer package. As a consequence of this, usual Bragg–Gray/Spencer–Attix theories cannot be applied with MV photon beams on account on the fact that the calculation of the dose inside the alumina crystal must take into account the electrons coming from the surroundings but also those resulting from photon interaction within the crystal.

We use the phenomenological model of Burlin [23] that provides a simple way to estimate the dose within the alumina crystal with respect to the dose in the surrounding media (mainly

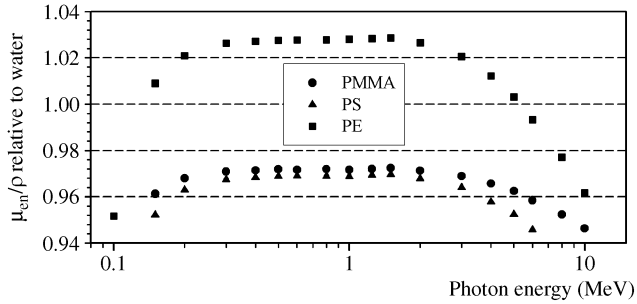


Fig. 8. Ratio of mass-attenuation coefficients for several polymers relative to water (data from NIST [24].

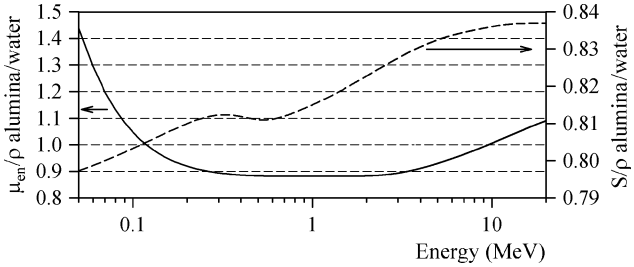


Fig. 9. Ratio of mass collision stopping power for alumina crystal relative to that of water with respect to electron energy (right) and ratio of mass-energy absorption coefficients for alumina relative to that of water with respect to photon energy (left). Data from NIST [24].

water). The Burlin model may be used because the surroundings and the alumina crystal are both of condensed states and a homogeneous photon field exists everywhere throughout water and the crystal. Electronic equilibrium is assumed within the alumina crystal.

The OSL sensors are packaged with polymers (mainly polyethylene (PE) of wall thickness $\sim$1 mm). Polymers (e.g., PE, PS, PMMA) are usually considered as good water-equivalent materials [22] and relative mass-attenuation coefficients of polymer relative to that of water exhibit a flat response in the medium-energy range (from 200 keV up to 3 MeV) as can be seen in Fig. 8.

Adapted to a LINAC beam, it means that water-equivalence may be assumed for reference energies up to 15 MV while the dose is underestimated for higher photon energies.

The Burlin model bridges the gap between the small cavity theory (Bragg–Gray) and the large cavity behavior. We introduce the dose ratio $f(E_i)$:

$$f(E_i) = d.\left(\frac{\left(\frac{S}{\rho}\right)_{\text{cryst}}}{\left(\frac{S}{\rho}\right)_{\text{water}}}\right) + (1-d).\left(\frac{\left(\frac{\mu_{\text{en}}}{\rho}\right)_{\text{cryst}}}{\left(\frac{\mu_{\text{en}}}{\rho}\right)_{\text{water}}}\right) \quad (3)$$

where $(S/\rho)_{\text{cryst}}$ and $(S/\rho)_{\text{water}}$ are mass collision stopping powers for alumina and water respectively and $(\mu_{\text{en}}/\rho)_{\text{cryst}}$ and $(\mu_{\text{en}}/\rho)_{\text{water}}$ are mass-energy absorption coefficients for the crystal and water, respectively.

Since secondary electrons degrade their energy from the starting energy $\overline{T}$ down to 0, the mean ratio of mass collision stopping power for the alumina crystal relative to that of water is calculated for the average electron energy $\overline{T}/2$ [22]. The ratio of mass-energy absorption coefficients is also calculated for all photon energies. For alumina, we used the following compound relation:

$$\left.\frac{\mu_{\text{en}}}{\rho}\right|_{\text{Al2O3}} = \left[(2.\text{A}_{\text{Al}}).\left.\frac{\mu_{\text{en}}}{\rho}\right|_{\text{Al}} + (3.\text{A}_{\text{O}}).\left.\frac{\mu_{\text{en}}}{\rho}\right|_{\text{O}}\right] / (2.\text{A}_{\text{Al}} + 3.A_{\text{O}}). \quad (4)$$

These data [24] are plotted in Fig. 9.

The d factor corresponds physically to the average value of the electron fluence reduction within the crystal. It approaches unity for a small crystal (no significant photon absorption) and zero for large ones. It is defined as [22], [23]

$$d = \left(1 - \exp(-\beta_{\text{Al2O3}}.L)\right) / \beta_{\text{Al2O3}}.L \quad (5)$$

where β_{Al2O3} is an effective absorption coefficient of electrons in the crystal. It is evaluated by using Burlin's suggested formula [23], modified as in [22]

$$\beta_{\text{Al2O3}}(cm^{-1}) = -\ln(0.04)/R \approx 3.219/R \quad (6)$$

where R (in cm) is defined as the maximum depth of electron penetration as may be estimated using the continuous slowing-down approximation (CSDA) table [21] for each average electron energy.

L (in cm) is the mean path length of the electrons across the crystal. Following [22], we pose

$$L = \frac{4.V}{S} \quad (7)$$

where V and S are the volume and the surface of the crystal, respectively. The TLD_{500} fiber crystal has a diameter of 1.4 mm and a length of 1.4 mm. The Landauer crystal is extracted from a brittle pellet. The mean path length L is about 0.1 cm for both crystals.

The absorption coefficient $\beta_{\text{Al2O3}}(\text{cm}^{-1})$ depends on electron energy T (MeV) according to the empirical relationship

$$\beta_{\text{Al2O3}} \approx \frac{8.65}{T^{1.82}} + \frac{16}{T^{0.9}}. \quad (8)$$

For each reference energy E_{ref}, we calculate the absorption coefficient and the Burlin d factor. The d factor is plotted on Fig. 10 over the energy spectrum of the LINAC (20 MV). One can see that it is below unity for all photon energies comprised within the LINAC spectrum, thus justifying the application of the Burlin's theory.

The Burlin equation was initially introduced for monoenergetic sources. Since the correction factor $\text{f}(E_i)$ depends on photon energy, it has to be evaluated over the whole LINAC photon spectrum $S(E_i)$. With this aim in view, the ratio of mass collision stopping powers and the ratio of mass-energy absorption coefficients for the crystal and water are also calculated for all photon energies (see Fig. 9).

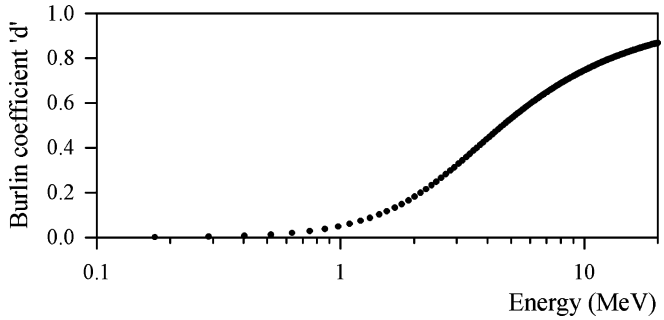


Fig. 10. Plot of the Burlin d factor versus photon energy (20 MV, $L = 0.1$ cm).

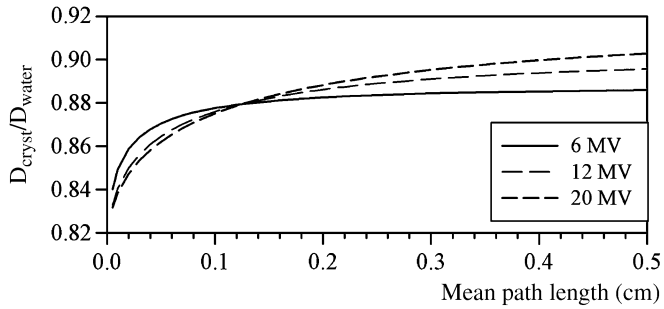


Fig. 11. Dose ratio $D_{\mathrm{cryst}}/D_{\mathrm{water}}$ with respect to mean path length L.

At the position of dose maximum within the water cube, where electronic equilibrium is achieved, the reference dose in water follows the photon fluence

$$D_{\mathrm{water}} = \int_0^{E_{\mathrm{ref}}} \left.\frac{\mu_{\mathrm{en}}(E_i)}{\rho}\right|_{\mathrm{water}} .S(E_i).dE_i \qquad (9)$$

Similarly, the dose in alumina can be estimated from the dose in water, using (3)

$$D_{\mathrm{cryst}} = \int_0^{E_{\mathrm{ref}}} \left.\frac{\mu_{\mathrm{en}}(E_i)}{\rho}\right|_{\mathrm{water}} .S(E_i).f(E_i).dE_i \qquad (10)$$

The dose ratio $D_{\mathrm{cryst}}/D_{\mathrm{water}}$ is then calculated from the (9) and (10) and plotted in Fig. 11 with respect to mean path length L.

One can see that energy independence may theoretically be obtained for L-value ~0.12 cm. This result calls for further experimental investigation as it is also LINAC-dependent.

The theoretical values of dose ratios $D_{\mathrm{cryst}}/D_{\mathrm{water}}$ are 0.8776, 0.8760, and 0.8752 for 6-MV, 12-MV, and 20-MV beams, respectively. The energy dependence for both OSL sensors is estimated by dividing the dose ratios by the value at 12 MV. The experimental tendencies are then compared to theoretical ones and quoted in Table III.

The agreement is satisfactory within experimental accuracy ($\sim \pm 0.2\%$) between 6 MV and 12 MV. Between 12 MV and 20 MV, however, the calculation underestimates the energy dependence, partly because the polymer package is no longer water-equivalent for this energy range (although an important part of secondary electrons actually comes from water).

TABLE III
ESTIMATION OF THE ENERGY DEPENDENCE FOR THE DOSE RATIO CRYSTAL/WATER VERSUS PHOTON ENERGY RANGE (RELATIVE TO THAT AT 12 MV)

Crystal type	OSL#3 (TLD_{500})		OSL#8 (Landauer)	
Energy range	6 – 12 MV	12 – 20 MV	6 – 12 MV	12 – 20 MV
Energy dependence *vs* water (theory)	1.002	0.999	1.002	0.999
Energy dependence *vs* water (experimental)	1.004	0.990	1.002	0.995

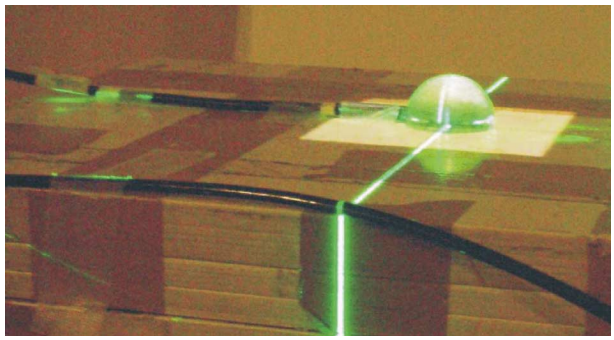


Fig. 12. Installation of the OSL sensor (OSL#3), equipped with its PMMA build-up cap, under the LINAC beam (courtesy IGR). The center of the cap is located by two crossed laser lines.

V. TESTS IN PRECLINICAL CONDITIONS WITH PHOTON BEAMS

A. Experimental

A build-up cap made of PolyMethylMetAcrylate (PMMA) was designed for electron beams at the reference energy of 12 MeV [15] using the Monte-Carlo code MCNP5 (Los Alamos National Laboratory, USA). It consists of a sphere (19 mm radius) cut in half. Seen from above, the OSL sensor is located at the center of the sphere but slightly offset from its center. Taking into account the density of PMMA (1.19 g/cm^3), the build-up cap is also suitable for 6-MV and 12-MV photon beams ($z_{\max} \sim 15$ mm and 25 mm in water, respectively).

The OSL/FO sensor mounted within its build-up cap was tested with an Oncor LINAC (Siemens OCS) at IGR (Fig. 12).

Beam energy was 6 MV, the field size (FS) was 10×10 cm^2 and the source–surface distance (SSD) was 100 cm. It is fixed onto a PS phantom and placed at the central axis of the beam. Half of the secondary electrons come from the phantom and the other half come from the PMMA build-up cap, both materials being nearly water-equivalent (Fig. 8).

Two experimental investigations were carried out with this set-up; the first is related to the field size dependence and the second one is related to angular dependence.

B. Dependence With Field Size (FS)

Although most part of the dose is delivered from the beam overlapping with the dosimeter, a significant amount of dose comes from the surroundings (secondary electrons and scattered photons). The dependence with FS is usually described by a relative output factor (OF) that is defined as the ratio of dose at one FS to that of a reference FS (usually 10×10 cm^2) for a given number of

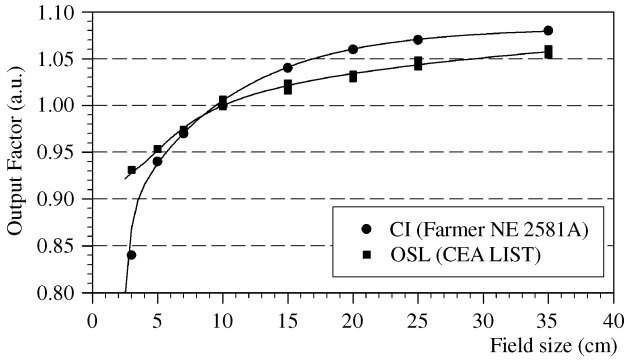


Fig. 13. Relative output factor for OSL/FO sensor and IC (response with field size normalized to that at reference field 10×10 cm^2).

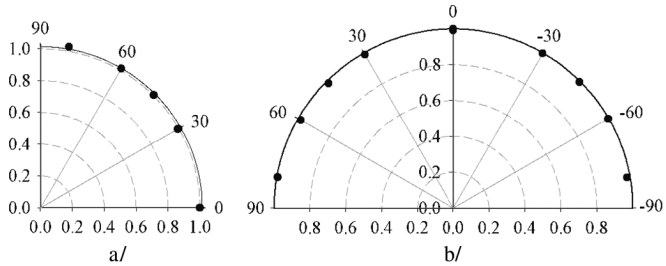


Fig. 14. Angular factor (AF) of the OSL sensor equipped with a PMMA build-up cap. a/ Evolution of the dose response as the OSL/FO sensor was oriented along gantry axis (θ study). b/ Evolution of the dose response as the OSL/FO sensor was placed within the rotation plane of gantry (ψ study).

monitor units (MU) and at normal incidence. The OF is depth-dependent and energy- and LINAC-dependent. Due to the wide variation in energy of scattered particles, the OF is also reliant on the energy response of the dosimeter with respect to water and thus is strongly dependent on dosimeter technology [25].

Practically, the dosimeter is calibrated in absorbed dose using a reference FS (e.g., 10×10 cm^2). In clinical use, however, the beam size and shape depend on the treatment. Consequently, the OF is measured for a given set of FS and shapes (e.g., square or circular) and the dosimeter signal is then corrected for OF influence to retrieve the dose value with arbitrary beam shape and size in clinical conditions.

A Farmer-type ionization chamber (NE 2581A) was used for comparison and placed under a 20-mm-thick PS sheet (same equivalent depth in water as for the OSL sensor). A square field was adjusted from 3×3 cm^2 up to 35×35 cm^2.

The OF has been estimated at normal incidence and is plotted in Fig. 13. One can see that FS dependence of the OSL sensor is smaller than that of the IC. This low dependence with FS is another asset of OSL technology as uncertainty in dose measurement due to FS variations is linked to the OF range.

C. Dependence With Beam Orientation

The OSL/FO sensor was first oriented along gantry axis (θ study) and the beam axis was moved from 0° (normal incidence) up to 80°. Then, the sensor was placed within the rotation plane of gantry (ψ study) and the beam axis was moved from $-80°$ up to 80°.

The angular factor (AF) is the relative dose response with respect to angular orientation of the beam for a constant amount of MU. It is plotted on Fig. 14 relative to normal incidence. One can see that the variations in AF are very small: $\sim \pm 1.5\%$ (θ study) and $\pm 0.9\%$ (ψ study). The residuals are of same order as repeatability ($\pm 1\%$) except for the θ study for which an unexpected dependence remains along fiber axis (2.5% at 80°) that is not well understood at the present time.

This quasi angular independence is also an asset for IVD in RT since it greatly simplifies the dosimetry.

VI. Conclusion

In vivo dosimetry (IVD), as part of the quality assurance during RT treatments, is now a legal requirement in several developed countries as ultimate safeguard against hypothetical accidents that may occur in case of improper TPS application.

For this purpose, online Al_2O_3:C OSL IVD with fiber optics brings a lot of advantages such as possibility of real-time monitoring of dose during treatment, high dose sensitivity, low energy and angular dependence, small size (IMRT, etc.), radiation hardness and low cost. Al_2O_3-OSL fiber sensing is also potentially attractive to save time at the dosimetry stage, to provide a quick assessment of delivered doses and to take suitable action in case of error in dose delivery.

In this paper, complementary investigations with photon beams are performed on Al_2O_3-OSL fiber sensors used with the multichannel OSL reader developed by the CEA LIST. Two alumina crystals are investigated [TLD_{500} (USTU) and Landauer] that are suitable for on line IVD. Sensor calibration and depth-dose measurements were performed with a Saturne 43 LINAC at CEA LIST LNHB. Calibration curves of OSL integrals show sublinear behavior accurately fitted by second-order equations.

The average energy dependence of the OSL sensor relative to water lies between 0.7% and 1.4%, depending on OSL sensors, over the energy range [6 MV, 20 MV]. This result shows that the high Z value of alumina ($\sim$11) relative to tissue is not an issue when performing dosimetry of MV photon and electron beams in RT. Relative mass-energy absorption coefficient and mass-collision stopping power of the crystal to that of water are taken into account to evaluate energy dependence for patient dosimetry in RT.

The dose within the alumina crystal is partly due to secondary electrons generated within water and polymer package and also to photon interaction within the crystal. Since the range of secondary electrons in the alumina crystal is of same order than its size, it cannot be considered as a "small" cavity. We adapted the phenomenological model of Burlin ("intermediate-size cavity") to a broadband LINAC photon spectrum in order to estimate the energy dependence of the OSL sensor in reference conditions. This model follows well experimental observations for the medium energy range [6 MV–12 MV]. For the high energy range [12 MV–20 MV], the calculation underestimates the energy dependence probably owing to the fact that the polymer package of the OSL sensor is no longer water-equivalent.

A PMMA build-up cap was designed for surface measurements. We show that it preserves energy and angular independence (AF) thus simplifying the dosimetry and exhibits a small

dependence with field size (OF) as well. However, it brings an important dose shadowing due to its large diameter that disturbs the isodose pattern with respect to the planned dose distribution and also results in skin over dosage over a large surface area. Since the dosimeters are not included into the TPS calculation, their placement into the beam affects the planned dose distribution although practically the dosimeters are not systematically used (only at the beginning of a new treatment). Build-up caps are most often made of metal (e.g., brass) in order to reduce the overexposed surface and the shadow-induced perturbations. In return, the dosimeter becomes energy-dependent and should be calibrated and used at a single energy. With this aim in view, an OSL sensor with a metallic build-up cap is also investigated along with tests in clinical conditions of the OSL unit and software at IGR.

ACKNOWLEDGMENT

S. Magne would like to thank Dominique Chambellan (CEA LIST DETECS-SSTM) for his assistance with the X-ray generator used for OSL testing, and Soizic Sorel and Aimé Ostroswky (CEA LIST LNHB) for their assistance with the LINAC Saturne 43.

REFERENCES

[1] O. Roy, S. Magne, J. C. Gaucher, L. Albert, L. Dusseau, J. C. Bessière, and P. Ferdinand, "All optical fiber sensor based on optically stimulated luminescence for radiation protection," presented at the 12th Int. Conf. Optical Fiber Sensor (OFS'97), Williamsburg, VA, Oct. 28–31, 1997.

[2] S. Magne and P. Ferdinand, "Fiber optic remote γ dosimeters based on optically stimulated luminescence: State-of-the-art at CEA," presented at the 11th Int. Congress Int. Radiation Protection Assoc. (IRPA 11), Madrid, Spain, May 23–28, 2004.

[3] M. S. Akselrod, V. S. Kortov, and E. A. Gorelova, "Preparation and properties of α-Al_2O_3:C," *Radiat. Prot. Dosim.*, vol. 47, pp. 159–164, 1993.

[4] G. Ranchoux, S. Magne, J. P. Bouvet, and P. Ferdinand, "Fibre remote optoelectronic gamma dosimetry based on optically stimulated luminescence of Al_2O_3:C," *Radiat. Prot. Dosim.*, vol. 100, pp. 255–260, 2002.

[5] J. Barthe, R. Hugon, and J. P. Nicolai, "MAESTRO: Methods and advanced equipment for simulation and treatments in radio-oncology," *Nucl. Instr. Phys. Res. A*, vol. 583, pp. 1–8, 2007.

[6] International Atomic Energy Agency (IAEA), "Absorbed dose determination in external beam radiotherapy: An international code of practice for dosimetry based on standards of absorbed dose to water," Vienna, Austria, IAEA Technical Report Series (TRS) 398, 2000.

[7] M. S. Akselrod, L. Botter-Jensen, and S. W. S. McKeever, "Optically stimulated luminescence and its use in medical dosimetry," *Radiat. Meas.*, vol. 41, pp. S78–S99, 2007.

[8] V. Schembri and B. J. M. Heijmen, "Optically stimulated Luminescence (OSL) of carbon-doped aluminum oxide (Al_2O_3:C) for film dosimetry in radiotherapy," *Med. Phys.*, vol. 34, pp. 2113–2118, 2007.

[9] P. A. Jursinic, "Characterization of optically stimulated luminescent dosimeters, OSLDs, for clinical dosimetric measurements," *Med. Phys.*, vol. 34, pp. 4594–4604, 2007.

[10] E. G. Yukihara, G. Mardirossian, M. Mirzasadeghi, S. Guduru, and S. Ahmad, "Evaluation of Al_2O_3:C Optically Stimulated Luminescence (OSL) dosimeters for passive dosimetry of high-energy photon and electron beams in radiotherapy," *Med. Phys.*, vol. 35, pp. 260–269, 2008.

[11] A. Viamonte, L. A. R. da Rosa, L. A. Buckley, A. Cherpak, and J. E. Cygler, "Radiotherapy dosimetry using a commercial OSL system," *Med. Phys.*, vol. 35, pp. 1261–1266, 2008.

[12] M. C. Aznar, C. E. Andersen, L. Botter-Jensen, S. A. J. Bäck, S. Mattsson, F. Kjaer-Kristoffersen, and J. Medin, "Real-time optical fibre luminescence dosimetry for radiotherapy: Physical characteristics and applications in photon beams," *Phys. Med. Biol.*, vol. 49, pp. 1655–1669, 2004.

[13] J. C. Polf, S. W. S. McKeever, M. S. Akselrod, and S. Holmstrom, "A real-time, fibre optic dosimetry system using Al_2O_3 fibres," *Radiat. Prot. Dosim.*, vol. 100, pp. 301–304, 2002.

[14] S. Magne, L. Auger, J. M. Bordy, L. de Carlan, A. Isambert, A. Bridier, P. Ferdinand, and J. Barthe, "Multichannel dosemeter and Al_2O_3:C optically stimulated luminescence fibre sensors for use in radiation therapy: Evaluation with electron beams," *Radiat. Prot. Dosim.*, vol. 131, pp. 93–99, 2008.

[15] S. Magne, L. De Carlan, S. Sorel, A. Isambert, A. Bridier, P. Ferdinand, and J. Barthe, "Multichannel OSL dosimetry for dose verification in radiotherapy," presented at the 12th Int. Congress Int. Radiation Protection Assoc. (IRPA 12), Buenos Aires, Argentina, Oct. 19–24, 2008.

[16] E. G. Yukihara, V. H. Whitley, S. W. S. Mc Keever, A. E. Akselrod, and M. S. Akselrod, "Effect of high-dose irradiation on the optically stimulated luminescence of Al_2O_3:C," *Radiat. Meas.*, vol. 38, pp. 317–330, 2004.

[17] D. Lo, J. L. Lawless, and R. Chen, "Superlinear dose dependence of high temperature thermoluminescence peaks of Al_2O_3:C," *Radiat. Prot. Dosim.*, vol. 119, pp. 71–74, 2006.

[18] L. Blazy-Aubignac, "Contrôle Qualité des systèmes de planification dosimétrique des traitements en radiothérapie externe au moyen du code Monte-Carlo Penelope," (in French) Ph.D. dissertation, Univ. Toulouse III, Toulouse, France, Sep. 4, 2007.

[19] F. H. Attix and W. C. Roesch, *Radiation Dosimetry*, 2nd ed. : Academic Press, 1968, vol. 1, Fundamentals.

[20] A. T. Nelms, "Graphs of Compton energy-angle relationship and the Klein-Nishina formula from 10 keV to 500 MeV," National Bureau of Standards (NBS), U.S. Dept. Commerce, Circular 542, Aug. 28, 1953.

[21] ESTAR Database Available From NIST. [Online]. Available: http://www.physics.nist.gov/PhysRefData/Star/Text/ESTAR.html

[22] A. S. Beddar, T. R. Mackie, and F. H. Attix, "Water-equivalent plastic scintillation detectors for high-energy beam dosimetry: I. Physical characteristics and theoretical considerations," *Phys. Med. Biol.*, vol. 137, pp. 1883–1900, 1992.

[23] T. E. Burlin, "A general theory of cavity ionization," *Br. J. Radiol.*, vol. 39, pp. 727–734, 1966.

[24] X-Ray Database Available From NIST. [Online]. Available: http://physics.nist.gov/PhysRefData/XrayMassCoef/cover.html

[25] M. Westermark, J. Arndt, B. Nilsson, and A. Brahme, "Comparative dosimetry in narrow high-energy photon beams," *Phys. Med. Biol.*, vol. 45, pp. 685–702, 2000.